

Some remarks on dipole showers and the DGLAP equationPeter Skands¹ and Stefan Weinzierl²¹*Theoretical Physics, Fermilab, MS 106, Box 500, Batavia, Illinois 60510, USA*²*Institut für Physik, Universität Mainz, D - 55099 Mainz, Germany*

(Received 13 March 2009; published 24 April 2009)

It has been argued recently that parton showers based on color dipoles conflict with collinear factorization and do not lead to the correct Dokshitzer-Gribov-Lipatov-Altarelli-Parisi (DGLAP) equation. We show that this conclusion is based on an inappropriate assumption, namely, the choice of the gluon energy as evolution variable. We further show numerically that Monte Carlo programs based on dipole showers with “infrared-sensible” evolution variables reproduce the DGLAP equation both in asymptotic form as well as in comparison to the leading behavior of second-order QCD matrix elements.

DOI: [10.1103/PhysRevD.79.074021](https://doi.org/10.1103/PhysRevD.79.074021)

PACS numbers: 13.87.Ce

I. INTRODUCTION

Because of the large center-of-mass (CM) energies at modern hadron colliders, and especially in connection with the production of high- \hat{s} states it is becoming increasingly essential that we have well-controlled calculations that cover all regions of phase space in a reliable way (see, e.g., [1]), and that these are implemented consistently in the phenomenological tools we use for collider studies—we shall here focus on Monte Carlo Event Generators. It is likewise important that we have an accurate theoretical understanding of the properties we rely on these calculations to have.

Nontrivial collider observables almost invariably involve an interplay between widely separated energy scales. This represents an important challenge to collider phenomenology since, in any gauge theory with massless gauge bosons (thus QED and QCD, in particular), such scale hierarchies give rise to logarithmic enhancements in the matrix elements, order by order in perturbation theory, which ultimately render a truncation of the perturbative series invalid at any fixed order. This becomes increasingly relevant as the collider CM energy (or other relevant hard scale) grows, leaving more room for scale hierarchies to develop beneath it.

A state-of-the-art collider physics calculation includes both a good description of physics at short distances—usually represented by perturbative leading order (LO) or next-to-leading order (NLO) matrix elements with renormalization-group (RGE) improved couplings—a good description of the transition from short to long distances, which takes proper account of any large scale hierarchies that may develop on the way—usually represented by leading-log (LL) parton showers incorporating as many next-to-leading-log (NLL) effects as feasible, as well as models of other possible perturbatively enhanced aspects such as multiple parton interactions (MPI)—and finally a good description of the physics at long distances—usually represented by nonperturbative models of beam remnants, hadronization, and hadron decays.

We shall here focus on parton shower algorithms, which provide the connection between the perturbative fixed-order matrix elements and the nonperturbative hadronization models, and which thus constitute an essential ingredient of general-purpose event generators like HERWIG [2,3], PYTHIA [4,5], or SHERPA [6].

Parton showers generate infinite-order approximations to matrix elements (both real and virtual), in such a way as to coincide exactly with the matrix elements in the singular limits. The number of singular coefficients that are reproduced exactly depends on the order of the parton shower; thus, an LL parton shower can be expected to generate the correct coefficients for the “leading” matrix-element singularities (to be defined further below). These terms dominate in the limit of infinitely large hierarchy between the scales of each successive emission, and hence LL showers are supposed to be exact in this so-called “strongly ordered” limit. An NLL shower [7–10] should also generate the correct coefficients for the next-to-leading singular terms (dominant in regions with one less large hierarchy than the strongly ordered limit), and so on. While the accuracy of the above mentioned general-purpose event generators can be debated, we note that none of them systematically include the tree-level $n \rightarrow n + 2$ and 1-loop $n \rightarrow n + 1$ splitting functions, and hence they are all formally LL. However, also without exception, they do incorporate a number of nontrivial NLL effects systematically and usually perform significantly better than corresponding analytical LL calculations. Any proposed algorithm should therefore be subjected to two basic tests: 1) whether it correctly reproduces QCD in the LL singular limit, and 2) how well it approximates QCD in NLL singular limits.

At first order in perturbation theory the matrix elements become singular in phase space regions corresponding to the emission of collinear or soft particles. The first showering algorithms started from the collinear factorization of the matrix elements and approximated color interference effects through angular ordering [11–13]. An alternative approach is the Lund-dipole or dipole-antenna shower

model, first implemented in ARIADNE [14–18], in which first-order color interference effects are instead taken into account by choosing color-connected *pairs* of partons to be the radiating entities.

Here, unfortunately, a digression on nomenclature is necessary. These parton pairs were simply called *dipoles* in the original Lund papers [14–18]. They are also known as antennae [19–21], mostly in fixed-order contexts. In order to be clear about what we mean to both communities, we therefore use the term *dipole-antennae* [22] here for these objects. Later, Catani and Seymour invented a related, but different, concept which they unfortunately also called dipoles [23]. Roughly, a Catani-Seymour dipole corresponds to one half of a dipole-antenna, partitioned in a way that isolates the collinear singularities; hence the Catani-Seymour dipole could also be called a *partitioned-dipole*, as suggested in [24]. The problem has been further compounded by a new generation of shower models based on Catani-Seymour dipoles being generally referred to as “dipole showers” [25–28], whereas the same name was already used by ARIADNE to describe its final-state radiation (FSR) model based on dipole-antennae [18]. To make the confusion complete, while ARIADNE’s algorithm for final-state radiation is based on a strict dipole-antenna picture, its treatment of initial-state radiation (ISR) is somewhat different. We shall nonetheless attempt to retain some measure of clarity by referring consistently to the Catani-Seymour-type as partitioned-dipoles and to the antenna-type as dipole-antennae. The two shower types do exhibit many similarities, so the distinction may mostly be important to experts, but as with all approximations, the devil is in the details.

The last few years have witnessed significant progress in the improvement of parton shower algorithms. Based on a proposal by Nagy and Soper [25,26] new algorithms based on partitioned-dipoles have been developed [27,28]. A new final-state algorithm relying on the dipole-antenna picture has also been constructed [22], with similar properties as the ARIADNE final-state shower, and a complete dipole-antenna shower model incorporating both ISR and FSR has been developed in [29]. These new algorithms have their origin in subtraction methods for fixed-order calculations [23,30–34] and implement in a correct way simultaneously the soft and the collinear limit in a manner similar to that of ARIADNE’s FSR model. At the same time the new partitioned-dipole algorithms (as well as any dipole-antenna algorithm) are able to satisfy simultaneously at each step momentum conservation and the on-shell conditions. This is possible, because they are based on $2 \rightarrow 3$ splittings, where the spectator can absorb the recoil. Within the traditional $1 \rightarrow 2$ splitting algorithms it is impossible to satisfy simultaneously momentum conservation and the on-shell conditions for a splitting. What has to be done in $1 \rightarrow 2$ splitting algorithms is either to restore momentum conservation by an *ad hoc* procedure in the

end, as in HERWIG, or to restore it more locally during the shower evolution, but still involving at least a third parton at each step, as in PYTHIA and SHERPA.

In a recent paper Dokshitzer and Marchesini [35] study a soft dipole-type model with recoil effects, which is obtained from considering multiple antennas in QCD [36]. The first version of Ref. [35] on the archive claimed that dipole showers are in conflict with collinear factorization and do not lead to the correct Dokshitzer-Gribov-Lipatov-Altarelli-Parisi (DGLAP) equation. Reference [35] motivated us to study this question in detail. In this paper we show that the above mentioned conclusion is a consequence of an inappropriate assumption, namely, the choice of the gluon energy as evolution variable. We further show that with a proper evolution variable the DGLAP equation is reproduced, thus proving that dipole showers, whether of the partitioned-type or the antenna-type, have the correct LL behavior, so long as sensible evolution variables are chosen. Subleading differences between these shower models will still be present, at the NLL level, which can first be accessed at 2nd order in perturbative QCD. We therefore also include a set of explicit comparisons of different shower models to 2nd order QCD matrix elements. We note that in a recent paper Nagy and Soper [37] have given a strict formal derivation that dipole showers reduce to the DGLAP equation in the strongly ordered limit. We further note that the second version of Ref. [35] on the archive only claims that models with the gluon energy as the evolution variable conflict with collinear factorization. This is in line with the findings of Ref. [37] and of this paper.

This paper is organized as follows: In Sec. II, we discuss the factorization of tree-level matrix elements in soft and collinear limits. In Sec. III, we review the way a parton shower is obtained from the factorization properties of the matrix elements. We discuss in detail the choice of the evolution variable and point out that an energy-ordered shower is not compatible with the collinear limit. Showers ordered by the transverse momentum or the virtuality are unproblematic. In Sec. IV, we consider the evolution of the nonsinglet quark fragmentation function. In Sec. V, we compare the analytical result of the previous section with numerical results obtained from Monte Carlo programs based on both partitioned-dipole and dipole-antenna showers. Again we show that, so long as “infrared-sensible” evolution variables are chosen, these showers correctly reproduce the collinear limit. Finally, Sec. VI contains our conclusions.

II. BASICS

To set the scene let us consider the matrix-element squared for $\gamma^* \rightarrow q(p_1)g(p_2)\bar{q}(p_3)$ in four dimensions:

$$|\mathcal{A}_3(p_1, p_2, p_3)|^2 = 8e^2 g^2 N_c C_F \left(2 \frac{s_{123}s_{13}}{s_{12}s_{23}} + \frac{s_{12}}{s_{23}} + \frac{s_{23}}{s_{12}} \right). \quad (1)$$

In this formula, e denotes the electromagnetic coupling, g denotes the strong coupling, $N_c = 3$ denotes the number of colors, and $C_F = (N_c^2 - 1)/(2N_c)$. The invariants are $s_{ij} = (p_i + p_j)^2$ and $s_{ijk} = (p_i + p_j + p_k)^2$.

In the limit where the momentum p_2 of the gluon becomes soft, the formula factorizes as

$$\lim_{p_2 \rightarrow 0} |\mathcal{A}_3(p_1, p_2, p_3)|^2 = 8\pi\alpha_s C_F \text{Eik}(p_1, p_2, p_3) \times |\mathcal{A}_2(p_1, p_3)|^2, \quad (2)$$

where

$$\text{Eik}(p_1, p_2, p_3) = 2 \frac{s_{13}}{s_{12}s_{23}}, \quad (3)$$

and $\alpha_s = g^2/(4\pi)$. The matrix-element squared for $\gamma^* \rightarrow q(p_1)\bar{q}(p_2)$ is given by

$$|\mathcal{A}_2(p_1, p_2)|^2 = 4e^2 N_c s_{12}. \quad (4)$$

In the limit where the momentum p_2 of the gluon becomes collinear with the momentum p_1 of the quark such that $p_1 = zP$ and $p_2 = (1-z)P$ we have the factorization

$$\lim_{p_1 \parallel p_2} |\mathcal{A}_3(p_1, p_2, p_3)|^2 = 8\pi\alpha_s C_F P_{q \rightarrow qg} |\mathcal{A}_2(P, p_3)|^2, \quad (5)$$

with the Altarelli-Parisi splitting function

$$P_{q \rightarrow qg} = \frac{1}{s_{12}} \left(\frac{2}{1-z} - (1+z) \right). \quad (6)$$

A similar factorization formula holds for the case where the gluon becomes collinear with the antiquark.

With the help of an antenna function [21,30] we may combine the three singular limits (p_2 soft, $p_2 \parallel p_1$ and $p_2 \parallel p_3$) into one formula:

$$\lim_{p_2 \text{ unresolved}} |\mathcal{A}_3(p_1, p_2, p_3)|^2 = 8\pi\alpha_s C_F A_3^0(p_1, p_2, p_3) \times |\mathcal{A}_2(\tilde{p}_1, \tilde{p}_3)|^2. \quad (7)$$

The antenna function is given by

$$A_3^0(p_1, p_2, p_3) = \frac{1}{s_{123}} \left(2 \frac{s_{13}s_{123}}{s_{12}s_{23}} + \frac{s_{12}}{s_{23}} + \frac{s_{23}}{s_{12}} \right), \quad (8)$$

which is exactly the object used in both ARIADNE and default VINCIA for $q\bar{q} \rightarrow qg\bar{q}$ branchings. The momenta \tilde{p}_1 and \tilde{p}_3 entering the matrix element \mathcal{A}_2 are obtained from p_1, p_2 and p_3 such that they approach the correct limit in all singular limits, one possibility is [30]

$$\begin{aligned} \tilde{p}_1 &= \frac{(1+\rho)s_{123} - 2rs_{23}}{2(s_{123} - s_{23})} p_1 + r p_2 \\ &\quad + \frac{(1-\rho)s_{123} - 2rs_{12}}{2(s_{123} - s_{12})} p_3, \\ \tilde{p}_3 &= \frac{(1-\rho)s_{123} - 2(1-r)s_{23}}{2(s_{123} - s_{23})} p_1 + (1-r)p_2 \\ &\quad + \frac{(1+\rho)s_{123} - 2(1-r)s_{12}}{2(s_{123} - s_{12})} p_3, \end{aligned} \quad (9)$$

where

$$r = \frac{s_{23}}{s_{12} + s_{23}}, \quad \rho = \sqrt{1 + 4r(1-r) \frac{s_{12}s_{23}}{s_{123}s_{13}}}. \quad (10)$$

Note that Eq. (7) gives the correct factorization in any singular limit: p_2 soft, $p_2 \parallel p_1$ and $p_2 \parallel p_3$. Let us introduce the dimensionless quantities

$$\begin{aligned} y_{12} &= \frac{s_{12}}{s_{123}} = 1 - x_3, & y_{23} &= \frac{s_{23}}{s_{123}} = 1 - x_1, \\ y_{13} &= \frac{s_{13}}{s_{123}} = 1 - x_2, \end{aligned} \quad (11)$$

where the x_i are the ordinary energy fractions, evaluated in the CM of the 3-parton system,

$$x_i = \frac{2E_i}{\sqrt{s_{123}}}. \quad (12)$$

Obviously we have $y_{12} + y_{23} + y_{13} = 1$ and $x_1 + x_2 + x_3 = 2$. The antenna function reads then

$$A_3^0(p_1, p_2, p_3) = \frac{1}{s_{123}} \left(2 \frac{y_{13}}{y_{12}y_{23}} + \frac{y_{12}}{y_{23}} + \frac{y_{23}}{y_{12}} \right). \quad (13)$$

The unresolved phase space in terms of these variables is

$$\begin{aligned} d\phi_{\text{unresolved}} &= \frac{s_{123}}{16\pi^2} dy_{12} dy_{23} dy_{13} \delta(1 - y_{12} + y_{23} + y_{13}) \\ &\quad \times \Theta(y_{12}) \Theta(y_{23}) \Theta(y_{13}). \end{aligned} \quad (14)$$

The Dalitz plot for the unresolved phase space is shown in Fig. 1. The allowed phase space consists of the triangle $y_{12} \geq 0, y_{23} \geq 0, y_{12} + y_{23} \leq 1$. The soft singularity cor-

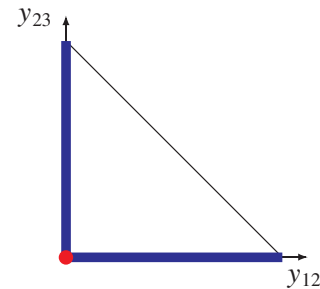


FIG. 1 (color online). The Dalitz plot for the phase space of the unresolved particle. The location of the soft singularity is shown by a dot, the location of the collinear singularities by a thick line.

responds to the point $y_{12} = y_{23} = 0$, while the collinear singularity $p_1 || p_2$ corresponds to the line $y_{12} = 0$ (and the collinear singularity $p_2 || p_3$ corresponds to the line $y_{23} = 0$).

We can write the antenna function A_3^0 in terms of two dipoles:

$$A_3^0(p_1, p_2, p_3) = D_{12,3} + D_{32,1}, \quad (15)$$

with

$$D_{12,3} = \frac{1}{s_{123}} \left(\frac{2y_{13}}{y_{12}(y_{12} + y_{32})} + \frac{y_{23}}{y_{12}} \right), \quad (16)$$

$$D_{32,1} = \frac{1}{s_{123}} \left(\frac{2y_{13}}{y_{23}(y_{12} + y_{23})} + \frac{y_{12}}{y_{23}} \right).$$

In their recent paper Dokshitzer and Marchesini [35] study a model consisting of only the soft part of the dipoles:

$$D_{12,3}^{\text{soft}} = \frac{2y_{13}}{y_{12}(y_{12} + y_{23})s_{123}}, \quad (17)$$

$$D_{32,1}^{\text{soft}} = \frac{2y_{13}}{y_{23}(y_{12} + y_{23})s_{123}}.$$

Dokshitzer and Marchesini actually use slightly different dipoles, obtained upon averaging over the azimuthal angle of the emitted particle around the emitter. The differences in the choice for the dipoles will not be relevant to the rest of the paper. Note that although we label these terms ‘‘soft,’’ the terms $D_{12,3}^{\text{soft}}$ and $D_{32,1}^{\text{soft}}$ have a soft and collinear singularity. It is also clear, that in the collinear limit $D_{12,3}^{\text{soft}}$ does not reduce to $P_{q \rightarrow qg}$, but to

$$P_{q \rightarrow qg}^{\text{soft}} = \frac{2z}{(1-z)s_{12}}. \quad (18)$$

In statements about shower algorithms reproducing the correct DGLAP equation in the collinear limit, the term ‘‘correct DGLAP equation’’ refers therefore for the model above to Eq. (18) and not to Eq. (6).

III. PARTON SHOWER

Whereas the factorization formula Eq. (7) is exact in all singular limits, the right-hand side of Eq. (7) does however not necessarily equal the full matrix element on the left-hand side away from the singular limit. (In the particular example discussed above the full matrix element for $\gamma^* \rightarrow qg\bar{q}$ actually equals the factorized form over the complete phase space, but this is not the general case.) Since for high parton multiplicities the full matrix elements are too complicated one approximates in a parton shower the full matrix elements by the factorized form over the complete phase space. Let us stress that this identification is exact in all singular limits and an approximation away from the singular limits.

The antenna function A_3^0 and the dipoles $D_{12,3}$ and $D_{32,1}$ are positive definite over the complete phase space and

therefore can be interpreted as a probability distribution for the emission of an additional particle. For a parton shower algorithm we introduce two variables t (‘‘shower time’’) and z (‘‘momentum fraction’’). The shower time t gives the scale at which the next splitting occurs, the variable z describes for a splitting $a \rightarrow bc$ the momentum fraction of the daughter b with respect to the mother a . For a complete description of a splitting we need in principle a third variable ϕ , but this variable will not be relevant for the discussion of this paper and we suppress it. Therefore we can restrict ourselves to a two-dimensional space parametrized by (t, z) or (y_{12}, y_{23}) as in Fig. 1. The choice for t (and z) is not unique. If we focus on the dipole $D_{12,3}$ with singularities for $s_{12} \rightarrow 0$ possible choices are

$$t_{\perp\bar{3}} = -\ln \frac{-k_{\perp}^2}{Q^2} = -\ln \left(\frac{y_{12}y_{23}y_{13}}{(1-y_{12})^2} \frac{s_{\bar{1}\bar{3}}}{Q^2} \right) \quad (19)$$

for a k_{\perp} -ordered shower or

$$t_{\bar{1}\bar{3}} = -\ln \frac{s_{12}}{Q^2} = -\ln \left(y_{12} \frac{s_{\bar{1}\bar{3}}}{Q^2} \right) \quad (20)$$

for a virtuality-ordered shower. The quantity Q^2 in Eqs. (19) and (20) is a fixed reference scale, usually taken to be the center-of-mass energy squared of the showering system. The shower time t takes values between a starting time t_0 and $+\infty$. As a larger values of t corresponds to lower scales we have to require that the singular region is contained in the region defined by $t \rightarrow \infty$. In Fig. 2, we show in the Dalitz plot lines of constant t for the definitions as in Eqs. (19) and (20). It is clear that the collinear singular region $y_{12} = 0$ is contained for both definitions in the region defined by $t \rightarrow \infty$.

Associated to the scale t is the Sudakov factor $\Delta_{12,3}$, giving the probability that no emission occurs between the scales t_0 and t

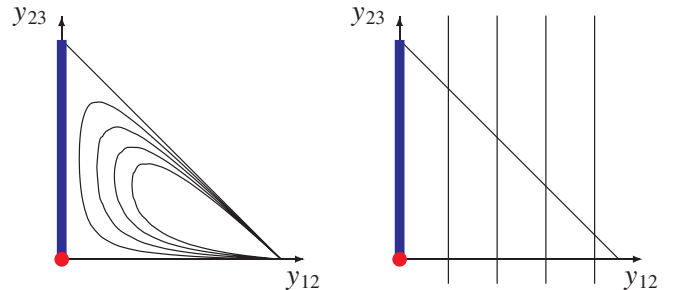


FIG. 2 (color online). Lines of constant shower time t for a k_{\perp} -ordered shower (left panel) and a virtuality-ordered shower (right panel). The singular region for the dipole $D_{12,3}$ is shown by a dot and a thick line. The singular region is approached for $t \rightarrow \infty$.

$$\Delta_{12,3}(t_0, t) = \exp\left(-\int_{t_0}^t dt' \int d\phi_{\text{unres}} \delta(t' - t_{\bar{1}\bar{3}})\right) \times 8\pi\alpha_s C_F D_{12,3}, \quad (21)$$

with $t_{\bar{1}\bar{3}}$ given by Eq. (19) or Eq. (20). The derivative of the Sudakov factor with respect to t gives the probability of a splitting at the shower time t :

$$-\frac{d}{dt}\Delta_{12,3}(t_0, t) = \frac{\alpha_s}{2\pi} C_F \int d\phi_{\text{unres}} \delta(t - t_{\bar{1}\bar{3}}) s_{123} D_{12,3}. \quad (22)$$

Working this out for a virtuality-ordered shower and setting $z = 1 - y_{23}$ one obtains

$$-\frac{d}{dt}\Delta_{12,3}(t_0, t) = \frac{\alpha_s}{2\pi} C_F \int_{\delta}^1 dz \left(\frac{2}{1-z+\delta} - 1 - z \right), \quad \delta = \frac{Q^2}{s_{\bar{1}\bar{3}}} e^{-t}. \quad (23)$$

At finite shower time t the splitting probability is finite, as it should be. In the limit $t \rightarrow \infty$ one recovers the DGLAP equation:

$$\lim_{t \rightarrow \infty} \left(-\frac{d}{dt}\Delta_{12,3}(t_0, t) \right) = \frac{\alpha_s}{2\pi} C_F \int_0^1 dz \left(\frac{2}{1-z} - 1 - z \right). \quad (24)$$

A similar analysis can be carried out for a k_{\perp} -ordered shower.

In their paper Dokshitzer and Marchesini [35] did not use the transverse momentum k_{\perp} or the virtuality as evolution variable. Instead they chose energy of the emitted gluon (in the rest frame of the dipole) as evolution variable. In our notation this amounts to the choice

$$t_{\bar{1}\bar{3}} = -\ln \frac{E_g^2}{Q^2} = -\ln \left(\frac{(y_{12} + y_{23})^2}{4} \frac{s_{\bar{1}\bar{3}}}{Q^2} \right). \quad (25)$$

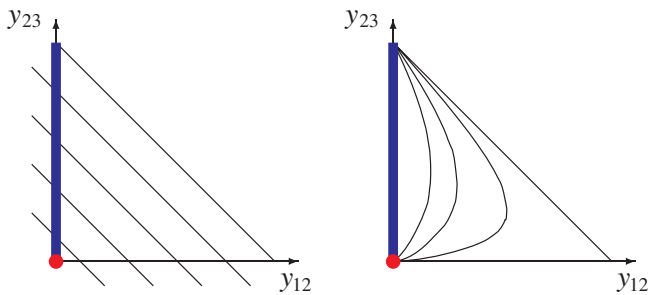


FIG. 3 (color online). Lines of constant shower time t for an energy-ordered shower (left panel) and an angular-ordered shower (right panel). The singular region for the dipole $D_{12,3}$ is shown by a dot and a thick line. For the energy-ordered shower, lines of constant t intersect the singular region for finite t . For the angular-ordered shower, the two singular points $(y_{12}, y_{23}) = (0, 0)$ and $(y_{12}, y_{23}) = (0, 1)$ are reached for finite shower time.

For this choice the lines of constant shower time t are shown in Fig. 3. In this case, $t \rightarrow \infty$ corresponds to the single point $y_{12} = y_{23} = 0$ in phase space and lines of constant t intersect the collinear region for finite t . We can therefore not expect to obtain a shower algorithm which is correct in the collinear limit based on this evolution variable. Indeed, a short calculation shows in this case

$$-\frac{d}{dt}\Delta_{12,3}(t_0, t) = \frac{\alpha_s}{2\pi} C_F \theta(1 - y_{\text{max}}) \int_0^{y_{\text{max}}} \frac{dy_{23}}{y_{\text{max}} - y_{23}} \times \left[1 - y_{\text{max}} \left(1 - \frac{1}{2} y_{23} \right) \right], \quad (26)$$

$$y_{\text{max}} = 2\sqrt{\frac{Q^2}{s_{\bar{1}\bar{3}}}} e^{-(t/2)}.$$

There are several problems related to an energy-ordered shower: For finite shower time t the splitting probability is infinite, due to the $1/(y_{\text{max}} - y_{23})$ singularity in the integrand. In the limit $t \rightarrow \infty$ the integration over y_{23} reduces to a point and not to the integral over the splitting function. The integrand of Eq. (26) bears no resemblance to the Altarelli-Parisi splitting function. These deficiencies are all related to the inappropriate choice of the shower evolution variable.

For completeness we also show the corresponding plot for an angular-ordered shower in Fig. 3. Lines of constant angle are given by

$$1 - \cos\theta_{12} = 2 \frac{y_{12}}{(y_{12} + y_{23})(1 - y_{23})} \quad (27)$$

and the corresponding definition of the shower time t is given by

$$t_{\bar{1}\bar{3}} = -\ln \left(\frac{y_{12}}{(y_{12} + y_{23})(1 - y_{23})} \frac{s_{\bar{1}\bar{3}}}{Q^2} \right). \quad (28)$$

The points $(y_{12}, y_{23}) = (0, 0)$ and $(y_{12}, y_{23}) = (0, 1)$ are also reached for finite shower time t and angular-ordered showers have to introduce a cutoff on the variable z to avoid these points. In more detail we have for an angular-ordered shower

$$-\frac{d}{dt}\Delta_{12,3}(t_0, t) = \frac{\alpha_s}{2\pi} C_F \theta(1 - y_{\text{max}}) \int_0^1 dy_{23} \times \left[2 \frac{1 - y_{23}}{y_{23}} \frac{1 - y_{\text{max}}}{1 - (1 - y_{23})y_{\text{max}}} + \frac{y_{23}}{1 - (1 - y_{23})y_{\text{max}}} \right], \quad (29)$$

$$y_{\text{max}} = \frac{Q^2}{s_{\bar{1}\bar{3}}} e^{-t}.$$

As already mentioned above, we have for an angular-ordered shower for finite t an infinite splitting probability due to the soft singularity at $y_{23} = 0$. In angular-ordered shower programs this situation is usually handled by introducing an *ad hoc* cutoff on the variable y_{23} . In the limit

$t \rightarrow \infty$ and setting $z = 1 - y_{23}$ we recover the DGLAP equation:

$$\lim_{t \rightarrow \infty} \left(-\frac{d}{dt} \Delta_{12,3}(t_0, t) \right) = \frac{\alpha_s}{2\pi} C_F \int_0^1 dz \left(\frac{2}{1-z} - 1 - z \right). \quad (30)$$

IV. THE NONSINGLET QUARK FRAGMENTATION FUNCTION

In this section, we review the relevant formulas for the evolution of the nonsinglet quark fragmentation function. The DGLAP evolution equation for the nonsinglet quark fragmentation function $d(x, Q^2)$ is

$$Q^2 \frac{d}{dQ^2} d(x, Q^2) = - \int_x^1 \frac{dz}{z} \frac{\alpha_s}{2\pi} C_F P_{qq}(z) d\left(\frac{x}{z}, Q^2\right), \quad (31)$$

where P_{qq} is the regularized splitting function

$$P_{qq}(z) = \frac{2}{1-z} \Big|_+ + \frac{3}{2} \delta(1-z) - (1+z). \quad (32)$$

To a function $f(x)$ we denote the Mellin transform by

$$\tilde{f}(N) = \int_0^1 dx x^{N-1} f(x). \quad (33)$$

In Mellin space the evolution equation for the nonsinglet quark fragmentation function factorizes:

$$Q^2 \frac{d}{dQ^2} \tilde{d}(N, Q^2) = -\frac{\alpha_s}{2\pi} C_F \tilde{P}_{qq}(N) \tilde{d}(N, Q^2), \quad (34)$$

with

$$\tilde{P}_{qq}(N) = -2S_1(N-1) + \frac{3}{2} - \frac{1}{N} - \frac{1}{N+1}. \quad (35)$$

$S_1(N-1)$ is the harmonic sum

$$S_1(N-1) = \sum_{j=1}^{N-1} \frac{1}{j}. \quad (36)$$

For large N , $S_1(N-1)$ diverges logarithmically. In Mellin space the evolution equation can be solved analytically

$$\tilde{d}(N, Q^2) = \left(1 + \frac{\alpha_s(Q_0)}{4\pi} \beta_0 \ln \frac{Q^2}{Q_0^2} \right)^{-(2/\beta_0) C_F \tilde{P}_{qq}(N)} \tilde{d}(N, Q_0^2), \quad (37)$$

where $\beta_0 = 11/3C_A - 4/3T_r N_f$ is the first coefficient of the beta-function. We are also interested in a toy model with $\alpha_s = \text{const}$, in this case the solution is given by

$$\tilde{d}(N, Q^2) = \left(\frac{Q^2}{Q_0^2} \right)^{-(\alpha_s/4\pi) 2C_F \tilde{P}_{qq}(N)} \tilde{d}(N, Q_0^2). \quad (38)$$

The initial condition

$$d(x, Q_0^2) = \delta(1-x) \quad (39)$$

corresponds in Mellin space to

$$\tilde{d}(N, Q_0^2) = 1. \quad (40)$$

Finally we are interested in the x -space result for the quark fragmentation function $d(x, Q^2)$ for values of x close to 1 and with $\alpha_s = \text{const}$. In this region only soft gluons have been emitted. With the ansatz [38]

$$d(x, Q^2) = A(Q^2)(1-x)^{B(Q^2)} \quad (41)$$

and neglecting terms which vanish in the limit $x \rightarrow 1$ one finds the equation

$$\frac{1}{A(Q^2)} \frac{dA(Q^2)}{d \ln Q^2} + \frac{\alpha_s C_F}{\pi} \left[\frac{3}{4} - \gamma_E - \psi(B(Q^2) + 1) \right] + \ln(1-x) \left[\frac{dB(Q^2)}{d \ln Q^2} + \frac{\alpha_s C_F}{\pi} \right] = 0. \quad (42)$$

The coefficient of $\ln(1-x)$ and the term independent of $\ln(1-x)$ have to vanish independently. With the initial condition Eq. (39) one then obtains

$$\begin{aligned} \ln d(x, Q^2) = & - \left[1 + \frac{\alpha_s C_F}{\pi} \ln \frac{Q^2}{Q_0^2} \right] \ln(1-x) \\ & - \frac{\alpha_s C_F}{\pi} \left(\frac{3}{4} - \gamma_E \right) \ln \frac{Q^2}{Q_0^2} \\ & - \ln \Gamma \left(-\frac{\alpha_s C_F}{\pi} \ln \frac{Q^2}{Q_0^2} \right). \end{aligned} \quad (43)$$

This solution is valid for

$$(1-x) \ll 1 \quad \text{and} \quad \frac{\alpha_s}{\pi} \ln \frac{1}{1-x} \ll 1. \quad (44)$$

V. NUMERICAL STUDIES

A. The quark fragmentation function

In this section, we study the quark energy distribution in Monte Carlo events obtained from a shower simulation, starting from the hard matrix element $e^+e^- \rightarrow q\bar{q}$. As center-of-mass energy we take $Q = m_Z$, unless indicated otherwise. The $(N-1)$ -th moment of the quark energy distribution at the scale Q_j is just

$$\tilde{d}(N, Q_j^2). \quad (45)$$

Our main interest is the comparison between the numerical shower program and the analytical result from the DGLAP equation. For this comparison it is sufficient to consider a toy model with $\alpha_s = \text{const}$. We set $\alpha_s = 0.1$. For the numerical result we first generate quark-antiquark events according to the hard matrix element, then start the shower at a scale Q_0 and run the shower to the lower scale Q_{IR} . For a k_{\perp} -ordered shower starting from a process at the center-of-mass energy Q the upper limit on Q_0 is given by

$Q_{0,\max} = Q/2$. We then calculate the energy fraction of the quark (additional quarks obtained from $g \rightarrow q\bar{q}$ splittings are not relevant to the discussion here):

$$x = \frac{2E_q}{Q}. \quad (46)$$

This defines a distribution in x . In addition, we can simultaneously bin the moments of this distribution.

We perform several comparisons between the numerical shower program and the analytical result from the DGLAP equation. In Mellin space the DGLAP equation is an ordinary differential equation and the numerical shower program has to reproduce this equation in the strongly ordered limit. Strongly ordered implies that the scale of successive emissions satisfy

$$\dots \gg Q_{j-1}^2 \gg Q_j^2 \gg Q_{j+1}^2 \gg \dots \quad (47)$$

We can ensure these conditions by starting the shower at a rather low scale $Q_0 = 2$ GeV and run the shower only for a short interval to $Q_{\text{IR}} = 1$ GeV. The low starting scale Q_0 ensures $Q^2 \gg Q_0^2$ and no emissions with a scale larger than Q_0 are generated. The short interval ensures that the number of events with two or more emissions is negligible and almost all events will have either zero or one shower emission. This is necessary since although in a shower successive emissions are ordered

$$\dots > Q_{j-1}^2 > Q_j^2 > Q_{j+1}^2 > \dots, \quad (48)$$

condition (48) does not exclude successive emissions to be of the same order $Q_j^2 = O(Q_{j-1}^2)$. Running the shower over the short interval from 2 to 1 GeV tests therefore if the emission of a single particle correctly approaches the DGLAP limit. Figure 4 shows for this case the comparison between the numerical shower program and the analytical solution Eq. (38). We observe an excellent agreement.

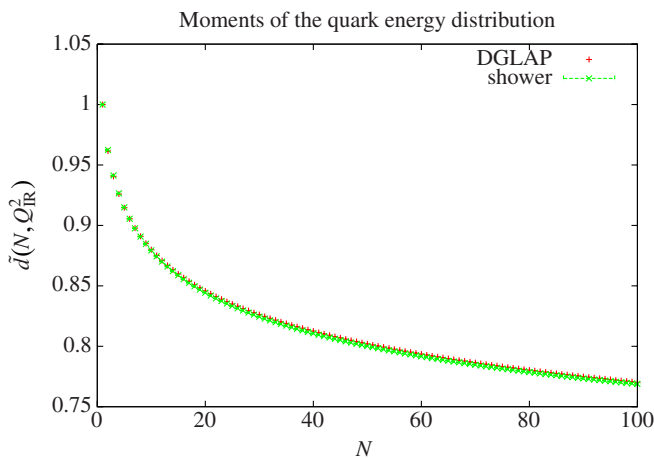


FIG. 4 (color online). Moments of the quark energy distribution at $Q_{\text{IR}} = 1$ GeV obtained from starting the evolution at $Q_0 = 2$ GeV.

We then compare the numerical shower program and the analytical result from the DGLAP equation for a larger interval for the evolution. We start the shower at the hard scale $Q_0 = Q_{0,\max}$ and run to the low scale $Q_{\text{IR}} = 1$ GeV. We compare again the moments of the quark energy distribution. We do this for the center-of-mass energies $Q = m_Z$, $Q = 1$ TeV, $Q = 10$ TeV, and $Q = 100$ TeV. We do not expect perfect agreement, since now the shower may generate emissions with a scale smaller but comparable to the previous one. However both the shower and the DGLAP equation resum the leading logarithm. In the limit where this logarithm is large against other terms, the results should agree. Figure 5 shows the comparison between the numerical shower program and the analytical solution Eq. (38) for the center-of-mass energies $Q = m_Z$, $Q = 1$ TeV, $Q = 10$ TeV, and $Q = 100$ TeV. The starting scale of the shower is always $Q_0 = Q_{0,\max} = Q/2$. For the final scale of the shower the value $Q_{\text{IR}} = 1$ GeV is always used. We observe that for large values of

$$\ln \frac{Q_0^2}{Q_{\text{IR}}^2} \quad (49)$$

the two results approach each other.

Figure 6 shows the 10th moment of the quark energy distribution as a function of the (fixed) value of α_s . The center-of-mass energy is $Q = m_Z$ and the starting scale of the shower $Q_0 = Q_{0,\max} = Q/2$. As the low scale $Q_{\text{IR}} = 1$ GeV is used. From Eq. (38) we expect on a logarithmic scale a linear relationship with respect to the variation of α_s :

$$\ln \tilde{d}(N, Q_{\text{IR}}^2) = -\frac{\alpha_s}{4\pi} 2C_F \tilde{P}_{qq}(N) \ln \frac{Q_0^2}{Q_{\text{IR}}^2}. \quad (50)$$

We observe in the left plot of Fig. 6 that both the numerical result from the shower program and the theoretical curve give straight lines. However the slope is slightly different. From Eq. (50) we see that the slope depends on the value of the hard scale Q_0 . To eliminate the dependence on Q_0 we show in the right plot of Fig. 6 the ratio $\tilde{d}(N, Q_{\text{IR}}^2)/\tilde{d}(N, 4Q_{\text{IR}}^2)$ of the 10th moment at the low scales Q_{IR} and $2Q_{\text{IR}}$. In this ratio the dependence on Q_0 drops out:

$$\ln \frac{\tilde{d}(N, Q_{\text{IR}}^2)}{\tilde{d}(N, 4Q_{\text{IR}}^2)} = \frac{\alpha_s}{\pi} C_F \tilde{P}_{qq}(N) \ln 2. \quad (51)$$

We observe an excellent agreement.

As a further comparison we now study the quark energy distribution in x -space for values of x close to 1. This region is sensitive to the emission of soft gluons. We start the shower at the hard scale $Q_0 = Q_{0,\max} = Q/2 = m_Z/2$, and use as the final scale of the shower $Q_{\text{IR}} = 1$ GeV. Figure 7 shows the comparison between the numerical shower program and the analytical solution Eq. (43). We observe a good agreement. We would like to make a comment: The analytical solution gives a linear relation

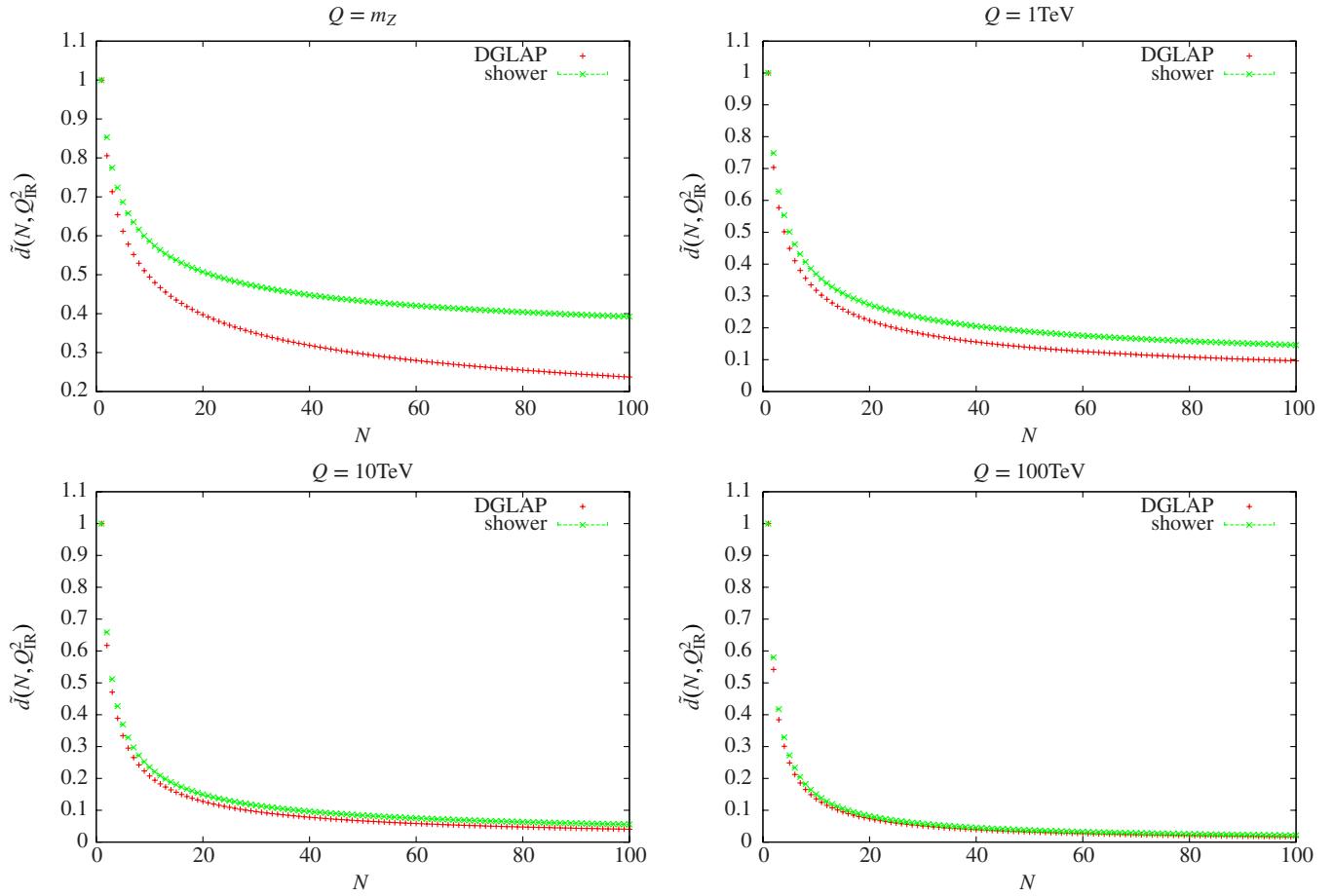


FIG. 5 (color online). Moments of the quark energy distribution at $Q_{\text{IR}} = 1 \text{ GeV}$ for various center-of-mass energies: $Q = m_Z$, $Q = 1 \text{ TeV}$, $Q = 10 \text{ TeV}$, and $Q = 100 \text{ TeV}$.

$$\ln d(x, Q^2) = A \ln(1 - x) + B, \quad (52)$$

the region

shown as a straight line in Fig. 7. The validity of the analytical solution according to Eq. (44) is restricted to

$$-\frac{\pi}{\alpha_s} \ll \ln(1 - x) \ll 0. \quad (53)$$

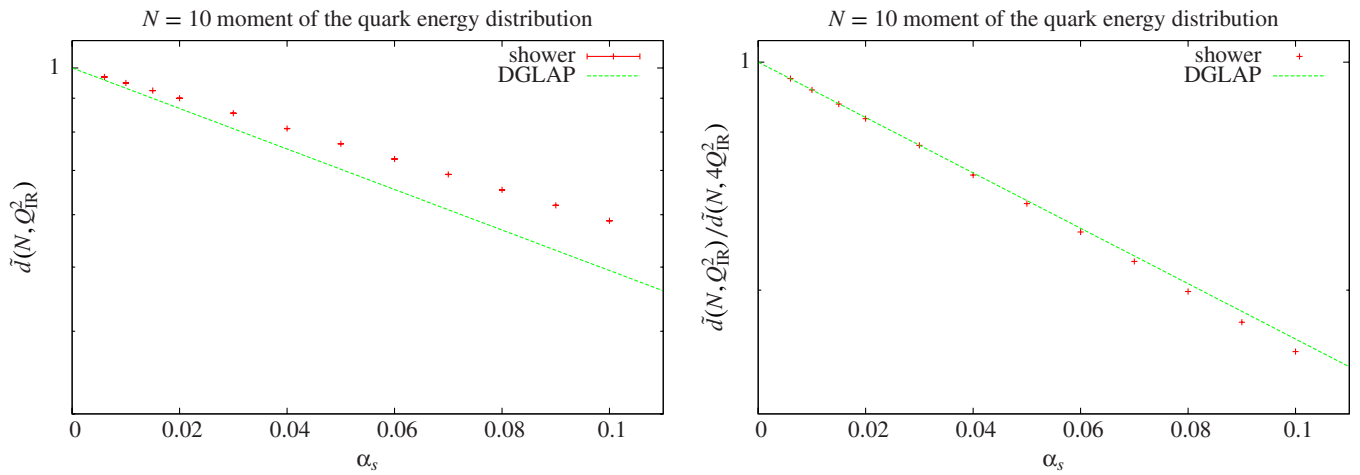


FIG. 6 (color online). The 10th moment of the quark energy distribution for various values of α_s , obtained from a process with center-of-mass energy $Q = m_Z$. The left figure shows the moment at $Q_{\text{IR}} = 1 \text{ GeV}$; the right figure shows the ratio between the values at $Q_{\text{IR}} = 1 \text{ GeV}$ and $Q_{\text{IR}} = 2 \text{ GeV}$.

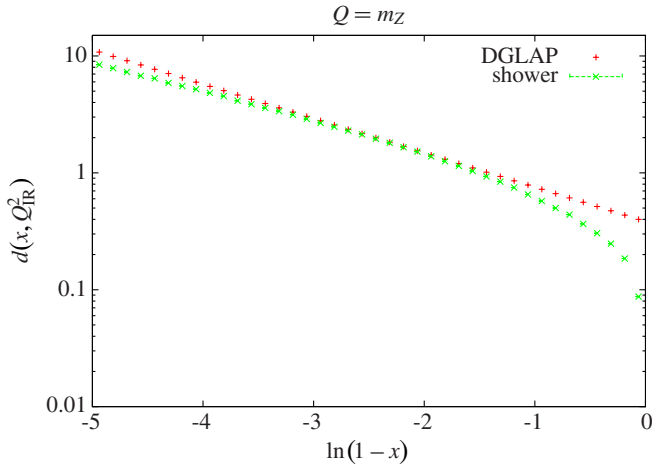


FIG. 7 (color online). The quark energy distribution for small values of $(1-x)$ at $Q_{\text{IR}} = 1$ GeV for the center-of-mass energy $Q = m_Z$.

Similarly, the shower does not generate emissions below a certain value of $\ln(1-x_{\text{max}})$. Values of $\ln(1-x)$ below that value would correspond to emissions with a scale less than Q_{IR} . As a consequence there are for any finite value of Q_{IR} events, which did not radiate at all. (The fraction of these events is determined by the Sudakov factor at the scale Q_{IR} .) In Fig. 7 we have normalized the shower result to the number of events which emitted at least one additional parton.

To further test the validity of our conclusions under systematic variations of the shower assumptions, we use the capabilities of the VINCIA plug-in to the PYTHIA 8 generator [5,22], which offers the possibility to use arbitrary radiation functions in conjunction with several different evolution variables within a dipole-antenna shower context. We also compare to the standard PYTHIA 8 p_{\perp} -ordered shower [39], which represents a hybrid between the parton and dipole approaches. In both programs, we switch off $g \rightarrow q\bar{q}$ branchings, use a fixed $\alpha_s = 0.1$ and take the starting scale to be $Q = 10^3$ GeV as default, with a hadronization scale (infrared cutoff) of $Q_{\text{IR}} = 1$ GeV. In VINCIA, we further switch off matching to matrix elements and matching to $2 \rightarrow 4$ antenna functions.

In VINCIA, we consider two different dipole-antenna evolution variables: transverse momentum (identical to the ARIADNE evolution variable [18]) and antenna-mass, referred to as type I and type II evolution, respectively. In terms of color-ordered triplets of parton momenta, these variables are defined as follows:

$$Q_{\text{I}}^2(p_1, p_2, p_3) = 4 \frac{s_{12}s_{23}}{s_{123}} \equiv 4p_{\perp}^2, \quad (54)$$

$$Q_{\text{II}}^2(p_1, p_2, p_3) = 2 \min(s_{12}, s_{23}) \equiv 2m_{\text{ant}}^2, \quad (55)$$

where the normalizations are chosen such that the maximal value of the evolution variable is s_{123} in both cases.

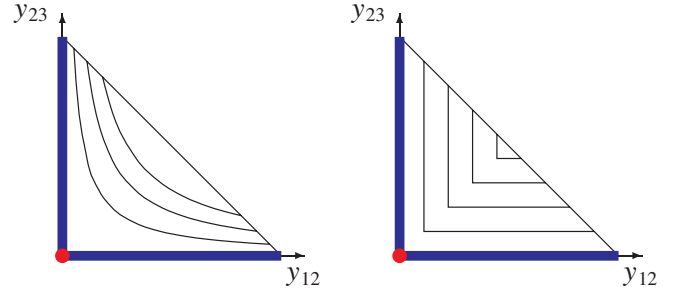


FIG. 8 (color online). Lines of constant shower time t for a p_{\perp} -ordered shower (left panel) and an antenna-mass-ordered shower (right panel). The singular region for the antenna $A(y_{12}, y_{23})$ is shown by a dot and a thick line. The singular region is approached for $t \rightarrow \infty$.

Contours for constant values of these variables are shown in Fig. 8.

The most general form for a leading-log antenna function (dipole-antenna splitting function) for massless parton splitting is represented by a double Laurent series in the two branching invariants [24],

$$A(y_{12}, y_{23}; s_{123}) = \frac{4\pi\alpha_s\mathcal{C}}{s_{123}} \sum_{\alpha,\beta=-1}^{\infty} C_{\alpha,\beta} y_{12}^{\alpha} y_{23}^{\beta}, \quad \text{with} \quad (56)$$

$$y_{ij} = \frac{s_{ij}}{s_{123}} \leq 1,$$

where \mathcal{C} is the color factor. We here consider 3 different choices for these functions, the Gehrmann-de-Ridder-Glover (GGG) ones [33], which are the defaults in VINCIA, and systematically high and low variations, min and max, respectively, with coefficients for the $q\bar{q} \rightarrow qg\bar{q}$ and $qg \rightarrow qgg$ functions given in Table I. We note that the default GGG $q\bar{q} \rightarrow qg\bar{q}$ function is identical to the corresponding function in ARIADNE and reproduces the $Z \rightarrow qg\bar{q}$ tree-level matrix element exactly. Also note that the color factor for $qg \rightarrow qgg$ is ambiguous up to $1/N_C^2$ and that this variation is included in the min/max variation.

In PYTHIA 8, the transverse-momentum variable, which we shall here call q_T to distinguish it from the other definitions, agrees with the ARIADNE definition in the infrared limit, but differs from it by up to a factor of 2 away from that limit; see [39]. The splitting functions in PYTHIA 8 are the ordinary DGLAP ones, augmented by matching to the tree-level $Z \rightarrow qg\bar{q}$ matrix element.

In this study, we do not include variations of the kinematics maps beyond that offered by the default PYTHIA 8 and VINCIA choices. PYTHIA 8 uses a partitioned-dipole-like map in which a “recoiler” recoils longitudinally (in the dipole center-of-mass frame) against a “radiator”. VINCIA by default uses the $gg \rightarrow ggg$ dipole-antenna map of ARIADNE for all branchings. In the dipole-antenna case, no special distinction is made between radiator and recoiler; instead the proper collinear limiting behavior is

TABLE I. Color factors \mathcal{C} (in the VINCIA normalization [22]) and Laurent coefficients $C_{\alpha,\beta}$ for the antennae used in this study. The coefficients with at least one negative index are universal (apart from a reparametrization ambiguity for gluons). The positive-index coefficients are arbitrary and are here varied between min and max.

	\mathcal{C}	$C_{-1,-1}$	$C_{-1,0}$	$C_{0,-1}$	$C_{-1,1}$	$C_{1,-1}$	$C_{-1,2}$	$C_{2,-1}$	$C_{0,0}$	$C_{1,0}$	$C_{0,1}$
GGG											
$q\bar{q} \rightarrow qg\bar{q}$	2	-2	-2	1	1	0	0	0	0	0	0
$qg \rightarrow qgg$	2	-2	-2	1	1	0	-1	2.5	-1	1.5	
Min											
$q\bar{q} \rightarrow qg\bar{q}$	2	-2	-2	1	1	0	0	-6	4.5	4.5	
$qg \rightarrow qgg$	2	-2	-2	1	1	0	-1	-8	8	7	
Max											
$q\bar{q} \rightarrow qg\bar{q}$	2	-2	-2	1	1	0	0	2	1.5	1.5	
$qg \rightarrow qgg$	2	-2	-2	1	1	0	-1	2	1.5	1.5	

obtained by a rotation angle going to 0° or 180° in the respective limits.

In Fig. 9, we show 4 plots illustrating the quark fragmentation function with these variations, as compared to the analytic expression, Eq. (43). The top left plot illustrates that one obtains good agreement between VINCIA and the analytic expression, irrespective of the choice of evolution variable. (Recall that the validity of the analytic expression is limited to the region $\ln(1-x) \ll 0$.) It should be noted, though, that it could still be possible to obtain bigger variations for more extreme variations of the choice of evolution variable. The top right plot illustrates the dependence on the choice of antenna functions. As expected, this variation is larger, since this dependence enters already at first order in the shower expansion. Nonetheless, the asymptotic slope of all the curves agrees with the analytic expectation. In the lower left-hand plot, we show the variation between PYTHIA 8 and VINCIA, with two different choices for the hadronization cutoff for the latter, either in p_\perp or in antenna mass. Though we emphasize that this distribution is very infrared sensitive, the dependence on the choice of hadronization cutoff here seems rather mild. The PYTHIA 8 curve has a slightly different slope than the VINCIA ones, but still appears to be within the uncertainty spanned by the variations above. Finally, in the lower right-hand plot, we show the results for two alternative starting scales, one at 100 GeV and the other at 10 000 GeV. As expected, the agreement improves with increasing energy (or, more precisely, with increasing Q_0/Q_{IR}).

In summary, we find no evidence in either partitioned-dipole or dipole-antenna showers of a breakdown of agreement with DGLAP-based predictions of the quark fragmentation function, provided that “infrared-sensible” evolution variables are chosen. The definition of infrared sensible is that both infinitely soft and collinear emissions should be classified as unresolved for any finite value of the evolution variable.

B. Comparison to second-order QCD

A complementary check on the accuracy of the shower can be obtained by comparing its second-order expansion to second-order QCD matrix elements. This is simplest for the dipole-antenna shower, for which the number of possible histories for each phase space point grows less fast than for the partitioned-dipole case, so in this subsection, we shall only use dipole-antenna showers for the comparisons, but we emphasize that the results should be qualitatively similar for the partitioned-dipole case. This part of our study is similar to a previous comparison of ARIADNE to second-order QCD by Andersson *et al.* [40].

In phase space regions dominated by leading logs, the ratio shower/matrix-element should be unity. In phase space regions dominated by hard wide-angle emissions, the shower could in principle be arbitrarily far from the matrix element, and finally in regions dominated by sub-leading logs (such as regions with two emissions at the same scale), the subleading-log properties of the shower can be probed.

To perform this test independently of the shower generator, we use RAMBO to generate a large number of evenly distributed 4-parton phase space points. For each phase space point, we evaluate the leading-color 4-parton antenna function,

$$A_{4\text{LC}} = \frac{|M_{4\text{LC}}(p_1, p_2, p_3, p_4)|^2}{|M_2(s)|^2}, \quad (57)$$

as given by Gehrmann *et al.* [33] (counter checked with [41] to protect against typos).

We then compute the tree-level leading-color LL antenna-shower approximation corresponding to the same phase space point, based on nested $2 \rightarrow 3$ branchings. For 4 partons, there are two possible antenna-shower histories:

- (i) In path A, parton 2 is emitted between partons 1 and 3. The 4-parton evolution scale is then $Q_{4A}^2 = Q_E^2(1, 2, 3)$.

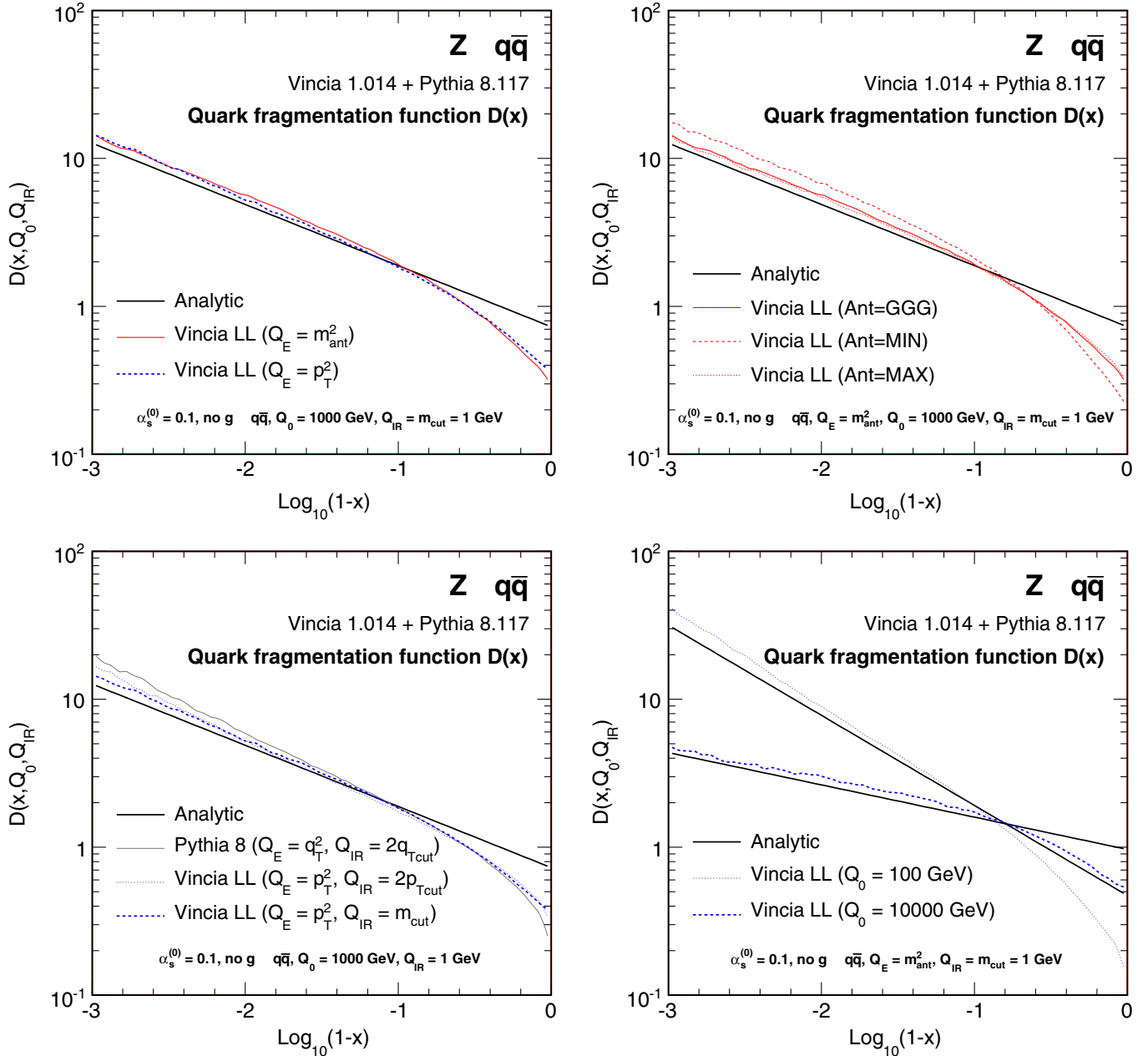


FIG. 9 (color online). The quark fragmentation function as obtained with VINCIA and PYTHIA 8, compared to the analytical expression, Eq. (43). *Top left panel*: variation of the evolution variable (p_{\perp} -ordering vs antenna-mass ordering). *Top right*: variation of the antenna functions (the Gehrman-Glover functions vs the VINCIA min and max variations). *Bottom left panel*: variation of the generator and of the hadronization cutoff contour (PYTHIA 8 vs p_{\perp} -ordered VINCIA with a cutoff in p_{\perp} or antenna-mass). *Bottom right panel*: variation of the starting scale ($m_Z = 10^2$ GeV vs $m_Z = 10^4$ GeV). In all cases, $g \rightarrow q\bar{q}$ branchings were switched off, a constant $\alpha_s = 0.1$ was used, and D was normalized to the number of inclusive 3-parton events at the cutoff.

- (ii) In path B, parton 3 is emitted between partons 2 and 4. The 4-parton evolution scale is then $Q_{4B}^2 = Q_E^2(2, 3, 4)$.

Q_E denotes a generic evolution variable. We shall here consider energy ordering, p_{\perp} -ordering, and antenna-mass ordering.

We note that a similar study for parton- or partitioned-dipole (Catani-Seymour) showers would need to consider 8

possible paths from 2 to 4 partons [42]: two possible radiators in the first $2 \rightarrow 3$ step (the quark and the anti-quark), and 4 possible radiators in the subsequent $3 \rightarrow 4$ step (treating the two “sides” of the gluon, which are generally associated with different kinematics mappings, as separate). The dipole-antenna shower is thus very economic in the number of terms generated at each successive order.

Using a new clustering algorithm that contains the inverse of the VINCIA $2 \rightarrow 3$ kinematics maps, we may perform clusterings of the type $(a, r, b) \rightarrow (\hat{a}, \hat{b})$ in a way that exactly reconstructs the intermediate 3-parton configurations that would have been part of the shower history for each 4-parton test configuration, for each of the paths A and B.¹ This gives us an exact tree-level reconstruction of how the antenna shower would have populated each path. We can now use this to test the shower approximation over all of 4-parton phase space.

We shall do this by plotting the ratio

$$R_4^0 = \frac{A_{q\bar{q}}(\widehat{12}, \widehat{23}, 4)A_{qg}(1, 2, 3) + A_{q\bar{q}}(1, \widehat{23}, \widehat{34})A_{g\bar{q}}(2, 3, 4)}{A_4(1, 2, 3, 4)}, \quad (58)$$

$$R_4^E = \frac{\Theta(Q_{3A} - Q_{4A})A_{q\bar{q}}(\widehat{12}, \widehat{23}, 4)A_{qg}(1, 2, 3) + \Theta(Q_{3B} - Q_{4B})A_{q\bar{q}}(1, \widehat{23}, \widehat{34})A_{g\bar{q}}(2, 3, 4)}{A_4(1, 2, 3, 4)}, \quad (59)$$

where

$$\begin{aligned} Q_{4A} &= Q_E(1, 2, 3); & Q_{3A} &= Q_E(\widehat{12}, \widehat{23}, 4) \\ Q_{4B} &= Q_E(2, 3, 4); & Q_{3B} &= Q_E(1, \widehat{23}, \widehat{34}). \end{aligned} \quad (60)$$

The ratio R_4^E now faithfully reproduces the shower approximation expanded to tree-level, phase space point by phase space point, for an arbitrary choice of evolution variable, Q_E .

Since the full 4-parton phase space has more dimensions than can fit on paper, and since the leading singularity of the gluon emission antenna functions goes like p_{\perp}^{-2} [with p_{\perp} defined as in Eq. (54)], we project the full phase space onto two p_{\perp} values, one of which we choose to correspond to the initial $2 \rightarrow 3$ step of a would-be shower history and the second to the $3 \rightarrow 4$ step. Specifically, the ordinate along the y axis will be

$$y \text{ axis: } p_{\perp;2} = \min(p_{\perp}(1, 2, 3), p_{\perp}(2, 3, 4)), \quad (61)$$

corresponding to the second branching, and the ordinate along the x axis will be the p_{\perp} value of the reclustered 3-parton configuration corresponding to the $\min(\dots)$,

$$x \text{ axis: } p_{\perp;1} = \begin{cases} p_{\perp}(\widehat{12}, \widehat{23}, 4) & ; p_{\perp}(1, 2, 3) < p_{\perp}(2, 3, 4) \\ p_{\perp}(1, \widehat{23}, \widehat{34}) & ; p_{\perp}(2, 3, 4) < p_{\perp}(1, 2, 3) \end{cases}. \quad (62)$$

Each point in $(p_{\perp;1}, p_{\perp;2})$ -space thus contains a distribution of all 4-parton configurations with that particular

¹Note that the inversion of VINCIA by this clustering algorithm is exactly one-to-one, with no approximation made. This was validated by reclustering a large number of actual branchings generated by the shower and recovering the prebranching configurations exactly, including global orientations, etc.

with hatted variables \hat{ij} denoting clustered momenta. R thus gives a direct measure of the amount of overcounting or undercounting by the shower approximation, with values greater than unity corresponding to overcounting and vice versa.

The ratio above, Eq. (58), contains nested products of antennae, identical to the subtraction terms that would be used in a fixed-order calculation. This does not take into account the ordering condition imposed in the shower, however. To impose this condition, we must include step functions in the shower approximation, as follows:

combination of $p_{\perp;1}$ and $p_{\perp;2}$ values. We shall plot both the average of this distribution, which we call $\langle R_4^E \rangle$, as well as a measure of the spread of the distribution, which we define as

$$\text{rms}(R_4^E) = 10^{\text{rms}(\log_{10}(R_4^E))} \geq 1. \quad (63)$$

By using this form we probe the average factor of deviation from unity rather than the absolute measure of the deviation itself. (I.e., we want a point with $R_4^E = 0.1$ to count as having a deviation of a factor of 10, rather than an absolute deviation of 0.9, from unity.) A special case is when we encounter dead zones in which the shower answer is zero, and hence the factor of deviation would nominally be infinite. When computing the rms above we therefore put a floor on the deviation at a factor 0.01 times the matrix element.

In Figs. 10 and 11, we show the average and rms for four different ordering variables; for comparison, we first show the result *without* any ordering imposed, as in Eq. (58), i.e., a simple product of nested antennae with no Θ functions imposed. This is equivalent to the subtraction terms constructed for fixed-order calculations and can be represented by “ordering” in the variable $m_{\text{max}}^2 = \max(s_{12}, s_{23})$. We then compare to the ordered results, Eq. (59), for energy ordering (as defined by Dokshitzer and Marchesini, i.e., ordering in the energy of the emitted parton in the CM of the Z boson), p_{\perp} -ordering [as defined in Eq. (54)], and antenna-mass ordering [as defined in Eq. (55)]. We may identify several regions of interest on the plots shown in Figs. 10 and 11:

- (i) *Origo*: double-LL singular region: $p_{\perp;2} \ll p_{\perp;1} \ll s$, i.e., two widely separated jets plus two strongly ordered emissions. Should be correctly described by any LL shower.

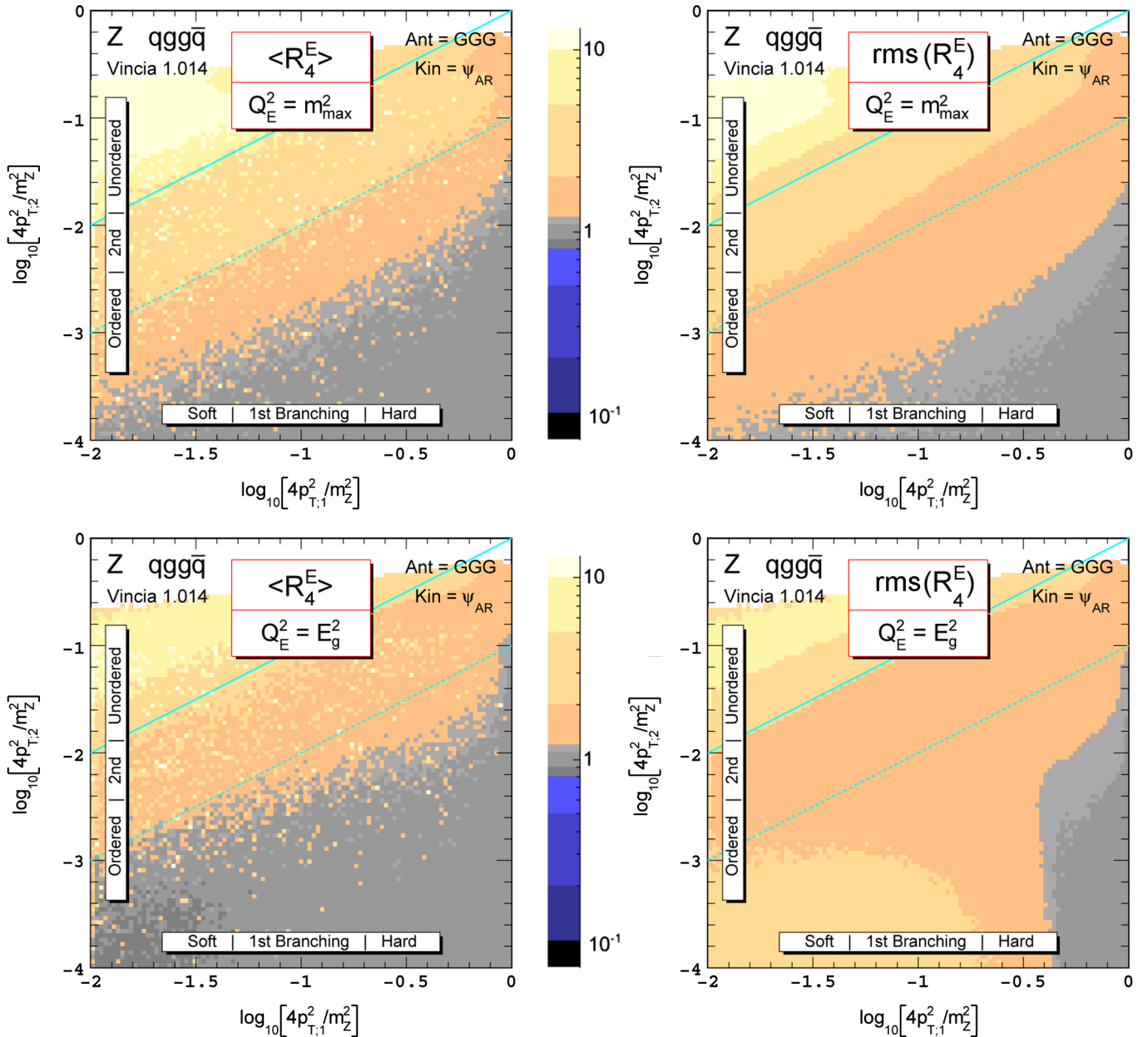


FIG. 10 (color online). *Left panels:* Average of the R_4^E distributions, Eqs. (58) and (59), for no ordering (*top*) and energy ordering (*bottom*). Diagonal lines indicate boundaries between unordered, ordered, and strongly ordered regions (doubly strongly ordered region is at origo). *Right panels:* the rms of the factor of deviation from unity of the R_4^E distributions.

- (ii) *Top right-hand corner:* Hard region: $p_{\perp,1} \sim p_{\perp,2} \sim s$, i.e., 4 widely separated jets. Should be correctly described only by the 4-parton matrix element.
- (iii) *Area below diagonal dashed (cyan) line (bottom right-hand corner):* region in which the second emission is strongly ordered with respect to the first: $p_{\perp,2} \ll p_{\perp,1}$. Should be correctly described by any LL shower matched to the 3-parton matrix element.
- (iv) *Intersection of y axis with diagonal solid (cyan) line:* Single-NLL (double-emission) region: $p_{\perp,2} \sim$

- $p_{\perp,1} \ll s$, i.e. 2 widely separated jets plus one strongly ordered $2 \rightarrow 4$ emission (two powers of α_s but only one large scale difference). Should be correctly described only by the 4-parton matrix element and/or by an NLL shower.
- (v) *Area above diagonal solid (cyan) line (except top right-hand corner; see above):* p_{\perp} -unordered region. Corresponds to a dead zone in a shower ordered in p_{\perp} . Although this zone occupies a relatively large area in our projection, this is chiefly an artifact of our choice of variables. The actual

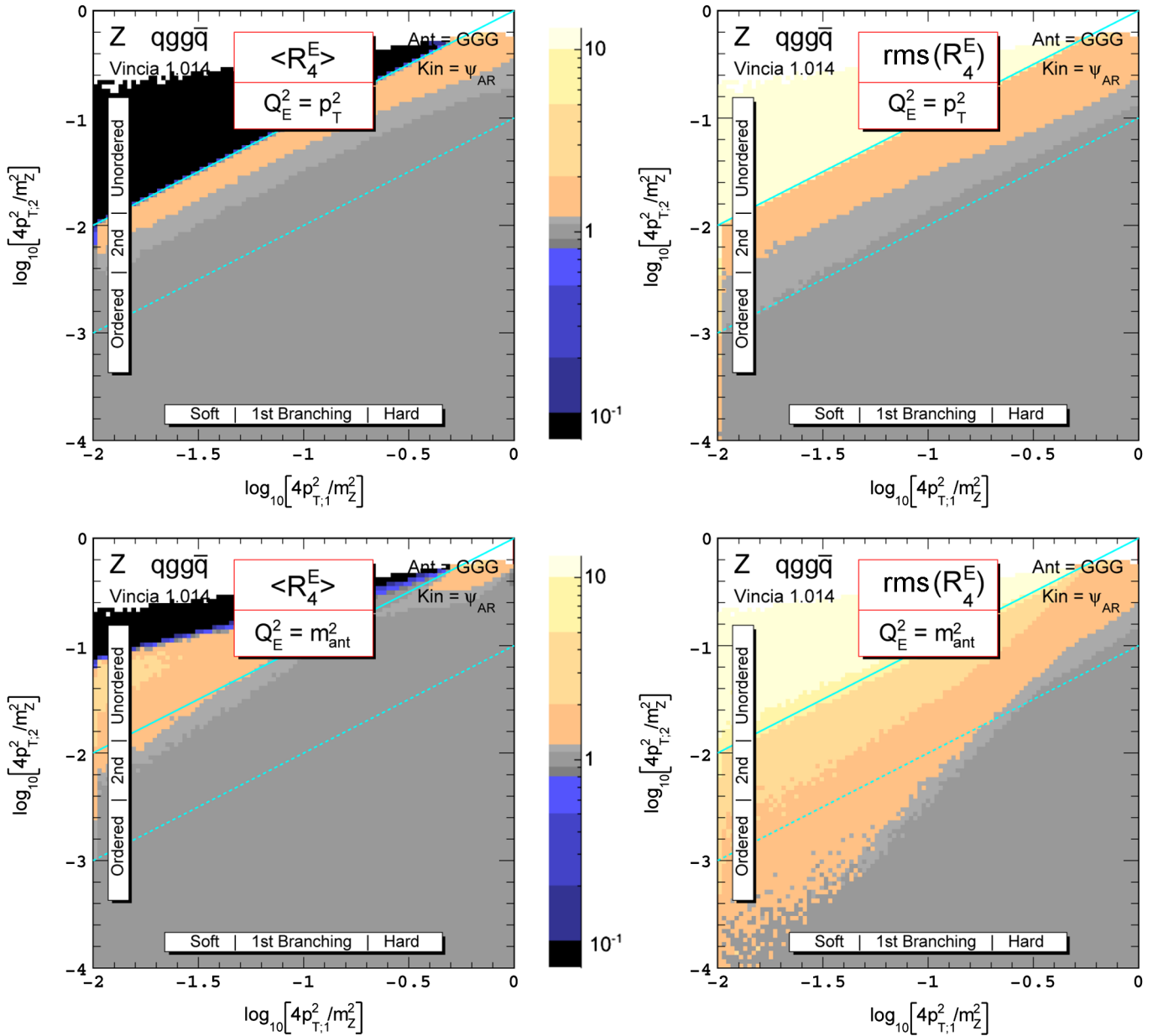


FIG. 11 (color online). *Left panels:* Average of the R_4^E distributions, Eq. (59), for p_{\perp} -ordering (top) and antenna-mass ordering (bottom). Diagonal lines indicate boundaries between unordered, ordered, and strongly ordered regions (doubly strongly ordered region is at origo). *Right panels:* the rms of the factor of deviation from unity of the R_4^E distributions. The rms distribution for antenna-mass ordering (on the lower right) is somewhat affected by the occurrence of a few dead points in a region extending towards the lower left, which artificially increase the rms in that region.

phase space volume in this region amounts to roughly 1.5% of the full 4-parton phase space.

Our operational definition of a “correctly described region” we shall here take to be that both the average of the R_4^E distribution as well as its rms factor in that region should tend to unity. If so, this means that the shower is not only getting the average of the distribution right, but there are also no large fluctuations on either side of the average. If only the average is unity but the rms factor is not, then the interpretation is that the shower is still over and under-

counting individual phase space points, and hence the relevant part of phase space is not being populated accurately.

In the top row of Fig. 10, we show the average and rms factor without imposing any ordering condition at all (apart from that implied by the nested phase spaces). The central grey color towards the bottom right indicates that the shower approximation deviates less than 10% from the matrix element there, and the two neighboring grey shades indicate 20% deviation. The next colors (lighter red and

darker blue shades) represent factors of 2, 5, and, 10, respectively. The dominance of light shades in the upper left half of the plots thus indicate that the nested LL antenna products, without ordering, exhibit a large overcounting whenever the 2nd emission does not have a p_{\perp} several orders of magnitude smaller than the 1st one.

As expected, the situation for energy ordering is actually worse (bottom plot row). Though the agreement improves slightly for hard 2nd emissions, we see a disturbing trend towards systematic undercounting in the double-LL region, indicated by the darkening shades towards origo. What is even more disturbing is that the rms factor does not follow the average, but instead blows up towards the LL singular regions. This means that the “good” average agreement on the left-hand side is really obtained by cancellations between large over and undercounting of individual phase space points. The desired LL singular behavior is therefore observed not to be obtained for this evolution variable.

Finally, the quite impressive properties of p_{\perp} -ordered dipole-antenna showers are evident in the near-unity average value of both R_4^E and its rms factor of deviation over all LL-dominated phase space regions in the top left-hand plot of Fig. 11, as was also noted in the study of Andersson *et al.* [40]. Though we here use a different set of antenna functions and kinematics maps, we see that the excellent basic agreement with the second-order QCD matrix elements is retrieved also in our case. We note that by definition a p_{\perp} -ordered shower does not generate any points in the p_{\perp} -unordered region above the diagonal (cyan) solid line. (Again, these dead zones were also pointed out in the study by Andersson *et al.* [40].) As mentioned, we find that roughly 1.5% of the full 4-parton phase space is left unpopulated by this particular ordering variable (antenna-mass ordering gives a similar number). Keep in mind that this is 4-parton space though; none of these showers have any dead zones in 3-parton phase space.

The case of antenna-mass ordering (Fig. 11, bottom row) is similar to p_{\perp} -ordering, but its dead zones do not follow strict contours of p_{\perp} , and hence the rms factor looks “artificially” large over that part of phase space in which dead points exist, roughly the area above the diagonal of the plot.

We plan to return to the issue of dead zones in a future paper, but note that since they are located in the NLL-dominated region, they do not affect the conclusions we wish to make here concerning the LL behavior of the evolution choices. We thus restrict ourselves to the conclusion that p_{\perp} -ordered dipole-antenna showers appear to give an excellent approximation to the full 4-parton matrix element over all LL-dominated regions of phase space [below the diagonal (cyan) dashed line]. When

p_{\perp} -ordering is imposed, the rms factor of deviation furthermore registers an impressive sharpening-up of the R_4^E distribution, yielding much larger regions of unity rms factor than the corresponding case without ordering. Also antenna-mass ordering represents a substantial improvement, although the improvement in the rms is slightly masked by the fact that our projection “smears out” its dead zones over a larger area of the plot than for p_{\perp} -ordering.

Energy ordering, on the other hand, effectively introduces artificially undercounted zones in the doubly-LL singular region, while still not removing the overcounting that was already present in the same region without ordering—hence the rms measure of deviation actually worsens as we go further into the singular region. The factorization implied by this choice of evolution variable is thus clearly not consistent with the structure of QCD.

VI. CONCLUSIONS

In this paper, we studied shower algorithms based on partitioned-dipoles and dipole-antennae. In particular we investigated the behavior in the collinear limit and showed that with an “infrared-sensible” definition of the evolution variable they reproduce the DGLAP evolution equation. The definition of infrared sensible is that both infinitely soft and collinear emissions should be classified as unresolved for any finite value of the evolution variable. Examples of such choices are k_{\perp} -ordering or mass ordering (ordering in virtuality for partitioned-dipole and antenna-mass for dipole-antenna showers, respectively). On the other hand, ordering in the energy of the emitted particle is not infrared sensible (it classifies infinitely collinear emissions as being resolved) and does not reproduce the DGLAP equation.

In addition to these analytic arguments, we have also presented a numerical study, making use of existing dipole shower algorithms. We demonstrated that the DGLAP behavior of the quark fragmentation function is reproduced by these models for a range of different infrared-sensible shower algorithms, in particular p_{\perp} -ordered ones. In addition we compared dipole-antennae to second-order QCD matrix elements and again retrieve good agreement in the strongly ordered (LL-dominated) region for p_{\perp} -ordering, but not for energy ordering.

ACKNOWLEDGMENTS

We would like to thank G. Gustafson, G. Marchesini, Z. Nagy and D. Soper for useful discussions. Special thanks go to H. Jung for organizing a discussion meeting at DESY.

- [1] J. Alwall, S. de Visscher, and F. Maltoni, *J. High Energy Phys.* 02 (2009) 017.
- [2] G. Corcella *et al.*, *J. High Energy Phys.* 01 (2001) 010.
- [3] M. Bähr *et al.*, *Eur. Phys. J. C* **58**, 639 (2008).
- [4] T. Sjöstrand, S. Mrenna, and P. Skands, *J. High Energy Phys.* 05 (2006) 026.
- [5] T. Sjöstrand, S. Mrenna, and P. Skands, *Comput. Phys. Commun.* **178**, 852 (2008).
- [6] T. Gleisberg *et al.*, *J. High Energy Phys.* 02 (2004) 056.
- [7] K. Kato and T. Muehisa, *Phys. Rev. D* **36**, 61 (1987).
- [8] K. Kato and T. Muehisa, *Phys. Rev. D* **39**, 156 (1989).
- [9] K. Kato and T. Muehisa, *Comput. Phys. Commun.* **64**, 67 (1991).
- [10] H. Tanaka, T. Sugiura, and Y. Wakabayashi, *Prog. Theor. Phys.* **114**, 477 (2005).
- [11] G. Marchesini and B.R. Webber, *Nucl. Phys.* **B238**, 1 (1984).
- [12] B.R. Webber, *Nucl. Phys.* **B238**, 492 (1984).
- [13] M. Bengtsson and T. Sjöstrand, *Phys. Lett. B* **185**, 435 (1987).
- [14] G. Gustafson, *Phys. Lett. B* **175**, 453 (1986).
- [15] G. Gustafson and U. Pettersson, *Nucl. Phys.* **B306**, 746 (1988).
- [16] B. Andersson, G. Gustafson, and L. Lönnblad, *Nucl. Phys.* **B339**, 393 (1990).
- [17] B. Andersson, G. Gustafson, L. Lönnblad, and U. Pettersson, *Z. Phys. C* **43**, 625 (1989).
- [18] L. Lönnblad, *Comput. Phys. Commun.* **71**, 15 (1992).
- [19] Y.I. Azimov, Y.L. Dokshitzer, V.A. Khoze, and S.I. Troyan, *Z. Phys. C* **27**, 65 (1985).
- [20] D.A. Kosower, *Phys. Rev. D* **57**, 5410 (1998).
- [21] J.M. Campbell, M.A. Cullen, and E.W.N. Glover, *Eur. Phys. J. C* **9**, 245 (1999).
- [22] W.T. Giele, D.A. Kosower, and P.Z. Skands, *Phys. Rev. D* **78**, 014026 (2008).
- [23] S. Catani and M.H. Seymour, *Nucl. Phys.* **B485**, 291 (1997).
- [24] Z. Bern *et al.* (NLO Multileg Working Group), arXiv:0803.0494.
- [25] Z. Nagy and D.E. Soper, *J. High Energy Phys.* 10 (2005) 024.
- [26] Z. Nagy and D.E. Soper, arXiv:hep-ph/0601021.
- [27] S. Schumann and F. Krauss, *J. High Energy Phys.* 03 (2008) 038.
- [28] M. Dinsdale, M. Ternick, and S. Weinzierl, *Phys. Rev. D* **76**, 094003 (2007).
- [29] J.-C. Winter and F. Krauss, *J. High Energy Phys.* 07 (2008) 040.
- [30] D.A. Kosower, *Phys. Rev. D* **57**, 5410 (1998).
- [31] L. Phaf and S. Weinzierl, *J. High Energy Phys.* 04 (2001) 006.
- [32] S. Catani, S. Dittmaier, M.H. Seymour, and Z. Trocsanyi, *Nucl. Phys.* **B627**, 189 (2002).
- [33] A. Gehrmann-De Ridder, T. Gehrmann, and E.W.N. Glover, *J. High Energy Phys.* 09 (2005) 056.
- [34] A. Daleo, T. Gehrmann, and D. Maitre, *J. High Energy Phys.* 04 (2007) 016.
- [35] Y.L. Dokshitzer and G. Marchesini, *J. High Energy Phys.* 03 (2009) 117.
- [36] A. Bassetto, M. Ciafaloni, and G. Marchesini, *Phys. Rep.* **100**, 201 (1983).
- [37] Z. Nagy and D.E. Soper, arXiv:0901.3587.
- [38] G. Altarelli, *Phys. Rep.* **81**, 1 (1982).
- [39] T. Sjöstrand and P.Z. Skands, *Eur. Phys. J. C* **39**, 129 (2005).
- [40] B. Andersson, G. Gustafson, and C. Sjögren, *Nucl. Phys.* **B380**, 391 (1992).
- [41] R.K. Ellis, D.A. Ross, and A.E. Terrano, *Nucl. Phys.* **B178**, 421 (1981).
- [42] S. Weinzierl, *J. High Energy Phys.* 03 (2003) 062.